ONLINE SUPPLEMENTAL MATERIAL

Supplemental Materials and Methods:

Preparation of 2D patterned substrates by microcontact printing.

The masters for PDMS molds were obtained by e-beam lithography and were designed with 1.0x1.0mm^2 regions of parallel lines 1.5 to 6μm wide with gaps of 3.5 to 20μm.

Glass coverslips #1.5 (Corning) were cleaned for 1h in a 3:1 concentrated H_2SO_4:30% H_2O_2 ("piranha") solution, rinsed with deionized water, and dried by rinsing in acetone and baking at 130ºC for 10min. 2.5nm of a 60/40 Au-Pd alloy was deposited on a 1.5nm Ti adhesion layer via e-beam evaporation using a Semicore SC2000 evaporator immediately after cleaning.

PDMS stamps were prepared using a Sylgard 184 silicone elastomer kit (Dow Corning) by pouring uncured elastomer over the master and curing overnight at 60ºC. The stamp was dipped in a 2mM ethanolic solution of HS-C_{18} thiol, dried with argon gas, and placed in contact with the substrate for 1min, after which the substrate was soaked for 2h in 2mM ethanolic solution of HS-$C_{11}EG_3$ thiol to render the non-stamped areas non-adhesive. Samples were rinsed with ethanol, dried with argon, and stored at 4ºC until the fibronectin coating.

One to five days prior to an experiment, substrates were incubated for 1.5h with 10μg/mL full-length fibronectin (Roche) at 37ºC and rinsed with PBS. Substrates are kept at 4ºC until use.

Preparation of 3D force-sensing pillared devices.

To measure traction forces produced by cellular bridges, we fabricated a PDMS-based flexible pillar device (Tan et al., 2003). We designed our device with an original geometry where 2μm diameter pillars are organized in rows separated by gaps of 10 or 15μm. Pillars are 5μm high and spaced 1μm away from each other within a row. We stamped the top of pillars with FN and passivated the rest of the surfaces with pluronic F-127 (Fig. S2). To

prevent collapse of force-sensing pillars, devices were unmolded in 70% ethanol solution. They were transferred in PBS and kept in liquid phase during the overall coating process.
Flat PDMS slabs were rendered hydrophilic by plasma cleaning (2mn) and coated with a FN solution (50μg/ml) in PBS for 15min. After rinsing PBS, they were gently pressed onto the pillars submerged in PBS. While in contact, we exchanged the PBS solution for a 0.1% pluronic F-127 in PBS and left for 1h to achieve passivation of the pillars' sides. Finally, we rinsed with PBS five times and remove the FN coated PDMS slabs. Before seeding the cells, we exchanged the PBS with cell culture solution (DME media with 10% FBS) and placed it at 37ºC in incubator.
Cells behavior was then followed by optical live-microscopy in order to measure traction forces produced by bridges. For scanning EM observations, cells were fixed with 3.7% formaldehyde in PBS for 20min, then dehydrated with successive baths in 50%–100% ethanol. They were critical point dried and coated with gold-palladium.

FRAP.

Confocal microscopy was performed with the confocal microscope FV500 Olympus. The bleaching was done on a 12x12μm^2 area, which included the actin bundles anchored to the FN stripes on the sides of the concave ends and spanning above the non-adhesive area toward the next adjacent stripe. The bleach region was scanned for 5.3s at low intensity for pre bleach intensity levels, then 3 times at full laser power for 2.3s and recovery images were taken every 30s at original intensity levels. The protocol we followed involved first a photo-bleaching of a cell (transfected with β-actin-GFP) and its recovery in presence of the vehicle media (ringer solution). Subsequently, we applied the MII-inhibitor BBI (50μM in ringer) to the same cell, for 3min (as the effect of BBI is visible after only 2min of drug application (Fig. 4 B)) just before washing out the drug and performing a new photo-bleaching. The fluorescence recovery was followed for not more than 10min (we noticed that the BBI effect lasted from 7 up to 10min after the drug removal (Fig. 4 B)). Such a protocol avoided the known phototoxicity of blue light in the presence of BBI (Sakamoto et

al., 2005) and allowed the MII-relaxing effect of the drug in the time frame of the observation. Quantification with recovery curves are displayed in Fig. S4.

Measure of the bridging index Br_i:

To determine the bridging efficiency of cells on FN stripes, we defined the bridging index Br_i as the ratio of the area of the cell in bridges (above PEG-passivated areas) on the total projected area of the cell: $Br_i = A_{BRIDGE}/A_{TOTAL}$. The total area of a cell is also the sum of the area of the cell in bridges and the area of the cell in contact with FN stripes: $A_{TOTAL} = A_{BRIDGE} + A_{FN}$. To calculate Br_i, we first measured the total area of cells. Helped by the fact that FN stripes can be detected by DIC microscopy, we easily measured the area of a given cell in contact with FN stripes. Then we calculate the Br_i for a cell as $(A_{TOTAL} - A_{FN}) / A_{TOTAL}$.

Myosin IIA knockdown experiment:

To determine if MIIA was a major player in the formation and maintenance of bridges, we transiently depleted MIIA in MEFs following the protocol developed earlier in our lab that ensures 85% reduction of protein levels (Cai et al., 2006). In a first set of experiments, MEFs were co-transfected with a plasmid encoding for a GFP (pmaxGFP from Lonza) and a plasmid (pSilencer H1-3.1 puro vector from Ambion, Austin) to express hairpin short interfering RNA (MIIA siRNA) targeting mouse non muscle MIIA (accession No. NM_022410). The targeting sequence is: GGTGAAGGTGAACAAGGAC. A control plasmid (Mock siRNA) encoding a hairpin siRNA whose sequence is not found in the mouse databases (provided by Ambion) was co-transfected with a plasmid encoding for mCherry in a second pool of MEFs. Transient transfection of plasmids was performed via electroporation. Cells were used 2 to 4 days after electroporation.

We plated together MIIA-depleted cells (GFP) and control cells (mCherry) onto continuous FN coated substrates as well as FN micropatterned substrates. After 30 min, cells were fixed and immunostained for MIIA. We first checked the efficiency of the MIIA depletion compared to control cells on continuous FN coated (Fig. S5). Levels of MIIA were significantly reduced in cells transfected with the plasmid MIIA siRNA (GFP labeled)

compared to untransfected cells or cells transfected with the Mock siRNA plasmid (mCherry labeled). To note, MIIA staining was similar in the two latter cases validating the Mock siRNA plasmid as an acceptable control condition.

When MIIA-depleted and control cells were plated for 30 min on substrates with FN stripes, cells from both conditions developed extensions on FN stripes very similar in length but MIIA-depleted cells develop no or smaller bridges than control cells as seen in Fig. S5. We also estimated the percentage of unspread cells as well as the percentages of spread cells displaying bridges and not displaying bridges for both MIIA-depleted and control cells. Control cells had a doubled population of cells with bridges after 30 min compared to the MIA-depleted ones (Fig. S5).

To understand such difference, we decided to follow the dynamics of spreading on FN stripes of MIIA-depleted cells. To do so, we used a plasmid MIIA siRNA-GFP expressing the same hairpin short interfering RNA targeting mouse non muscle MIIA and a GFP permitting to detect the MIIA-depleted cells. When MIIA-depleted cells spread on patterned substrates (Video 15), they developed smaller bridges and the bridging index plateaued after the first 30 minutes ($Br_i = 0.34$) whereas control cells spread with a constant bridging index ($Br_i = 0.58$, for FN lines of 4.15 μm, gaps of 18.8 μm) (Fig. 7 C). An interesting observation was that extensions on FN stripes in both control and MIIA knockdown cells were very similar (extension speed: 3.8 μm/min). However, MIIA-depleted cells were not able to expand bridges with the cellular extensions on FN stripes as in control cells (Fig. 2 B). Such results indicated that extension relied on a MIIA-mediated contraction of the actomyosin meshwork in the concave edge regions, pulling bridges forward along the FN stripes.

Supplemental figures:

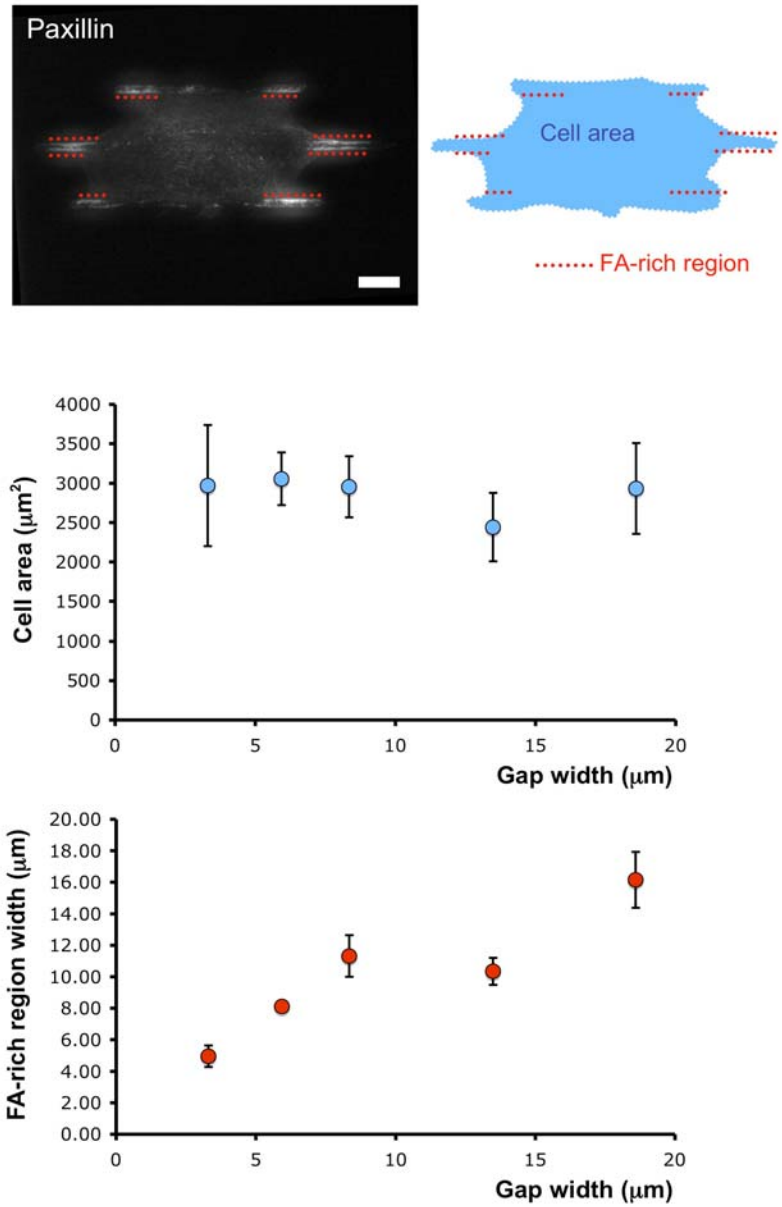

FIGURE S1: **Width of adhesion-rich regions adjacent to concave edges of bridges increased in size with the width of the non-adhesive gaps while total spread area was independent of it.** Top panel: Fluorescence image of FAs sites in a MEF where paxillin was labelled by immunostaining (left); Schematic drawing of the same cell with the total cell area in blue and the width of FA-rich regions adjacent to the concave edges of bridges in dashed red lines. Middle and bottom panels: Plots of the total cell area (blue circles, standard deviation, n = 3 to 14 cells per pattern) and of the width of FA-rich regions (red circles, standard deviation, n = 59 to 114 FA-rich regions per pattern) for MEFs spread for 90 min on patterned substrates vs. non-adhesive gap width of used patterns. Scale bar: 15 μm.

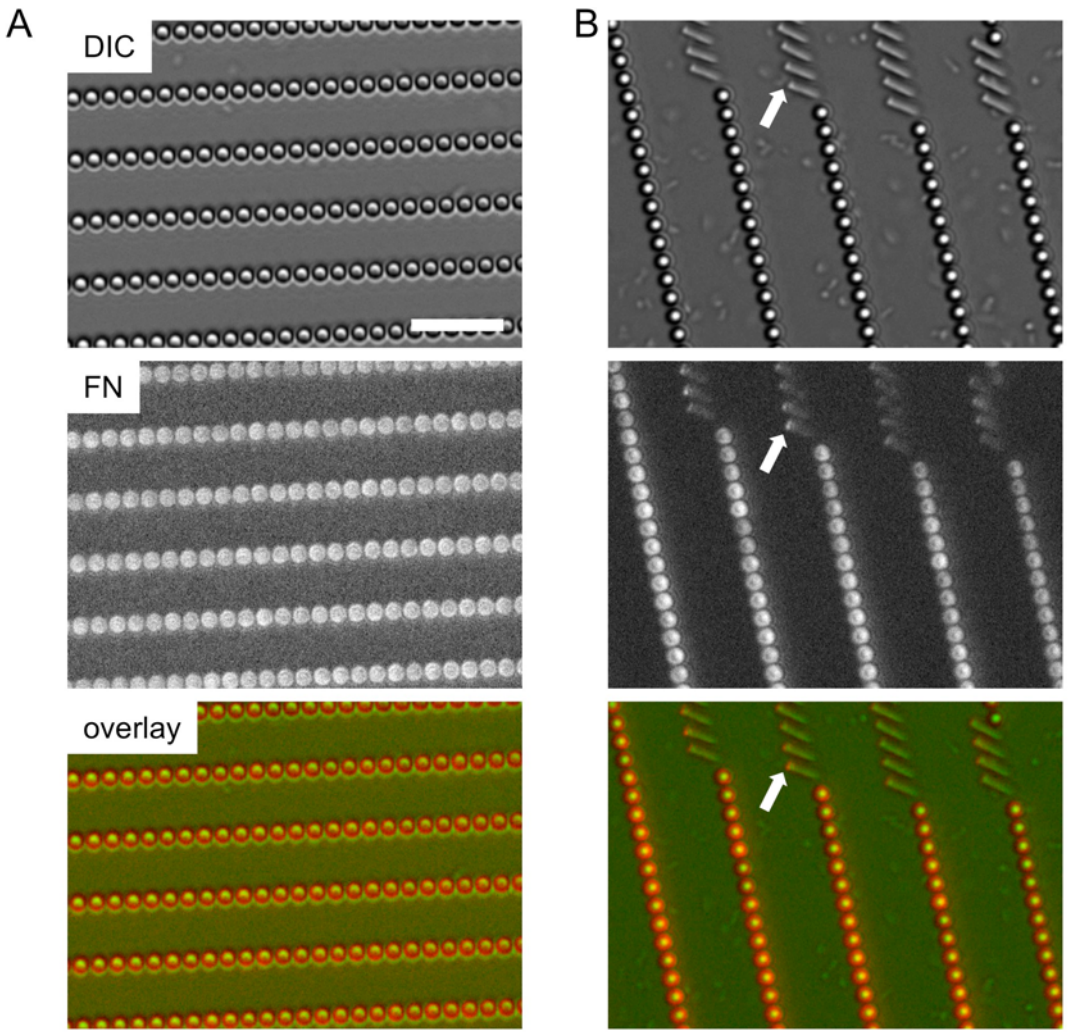

FIGURE S2: **Stamping of the top of the pillars with FN and blocking of their sides with pluronic F-127**. **(A),** Fluorescence micrograph of pillars' tips stamped with fluorescently labelled-FN blocked adhesion to their sides with pluronic F-127. **(B),** Fluorescence micrograph of pillars' tips stamped with fluorescently labelled-FN blocked adhesion to their sides with pluronic F-127. In the micrograph, some pillars collapsed after stamping. Fluorescence signal on such pillars is limited to the tips of the pillars (white arrow). Scale bar: 15 μm.

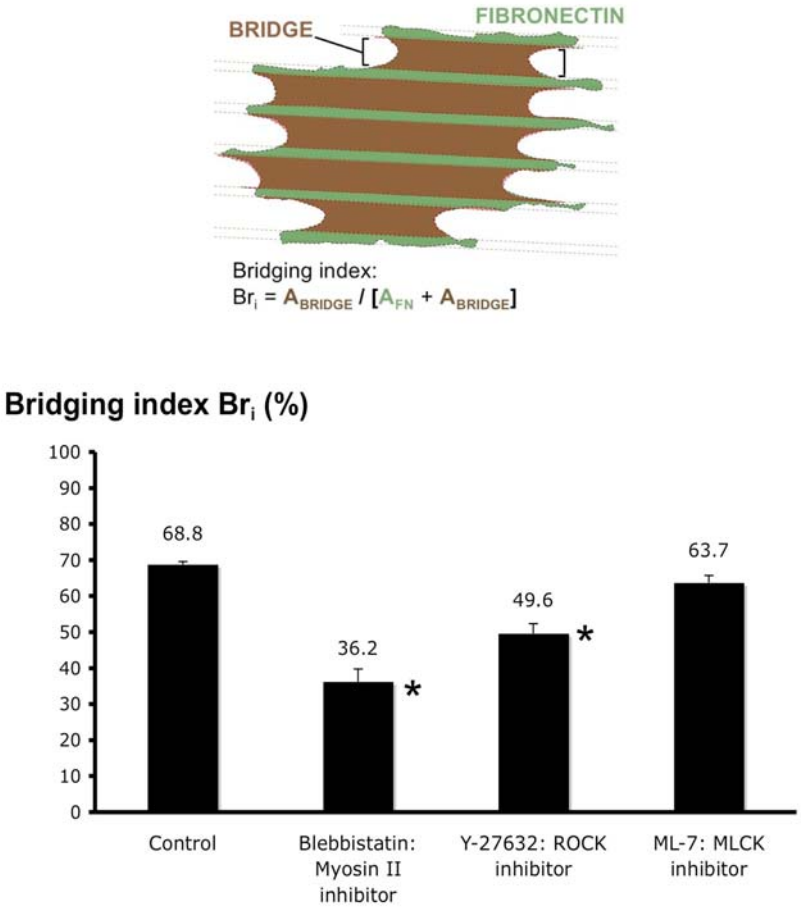

FIGURE S3: **Bridging index Br$_i$ of cells after direct and indirect myosin inhibition.** Bar chart of cells bridging index for a given pattern (FN 3.8 μm, gap 18.6 μm) after 90 min of different MII inhibition (BBI, ROCK inhibitor, MLCK inhibitor). Asterisks denotes when level of significance of a statistical difference was < 0.01.

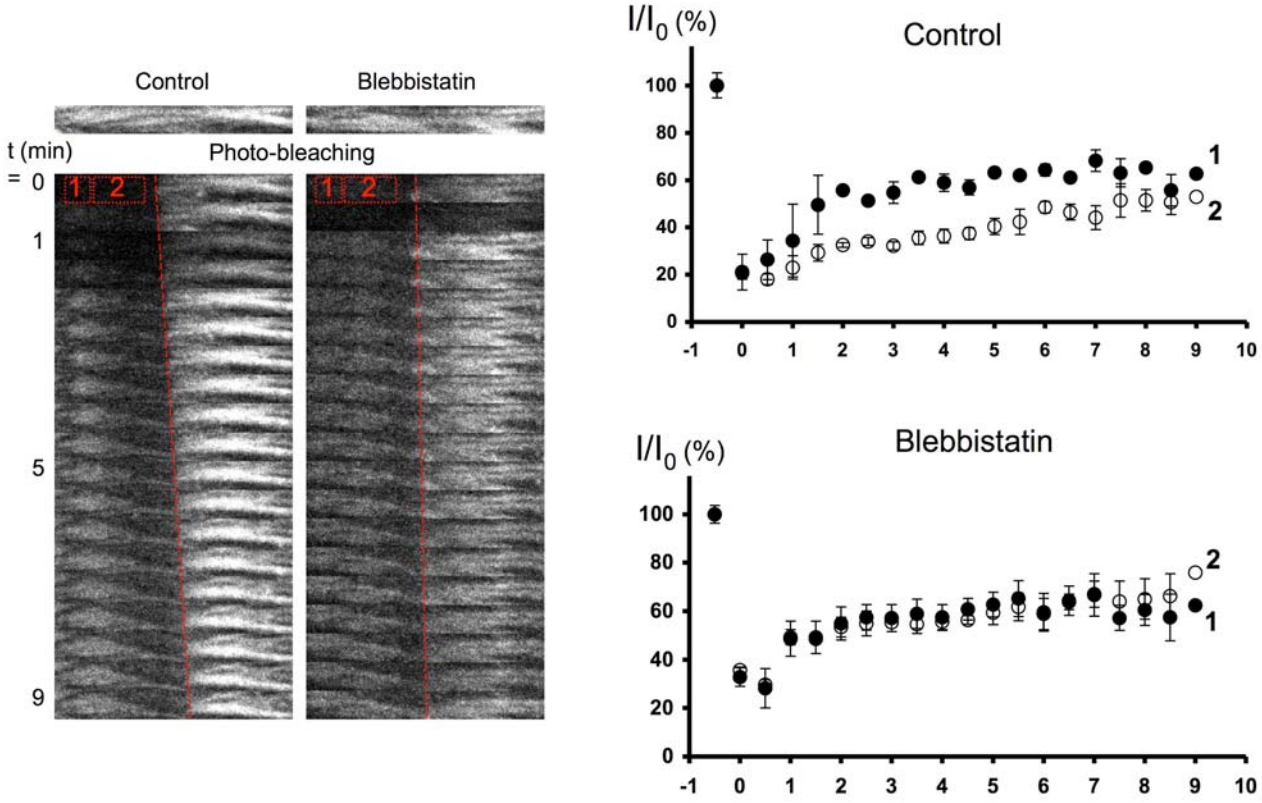

FIGURE S4: **FRAP recovery curves.** GFP-β-actin in region 1, was photobleached in a square of 12μm side (white square with dashed lines) in the same cell for two different conditions: control and BBI. Left: Montage of the actin bundles inside rectangles (15.2μm x 1.8μm) for the two conditions taken from Figure 5. Right: recovery curves for the two cases. We defined two different zones within the photo-bleached actin bundles: a zone comprising FAs (zone 1: closed circles) and another further away from the FAs (zone 2: open circles). When the recovery is happening homogeneously as during the BBI case without directed elongation from the adhesive area, recoveries in zones 1 and 2 are similar. When you add the force-dependent localized growth from FA as in the control case, recovery is faster in zone 1 compare to zone 2. Error bars are sd.

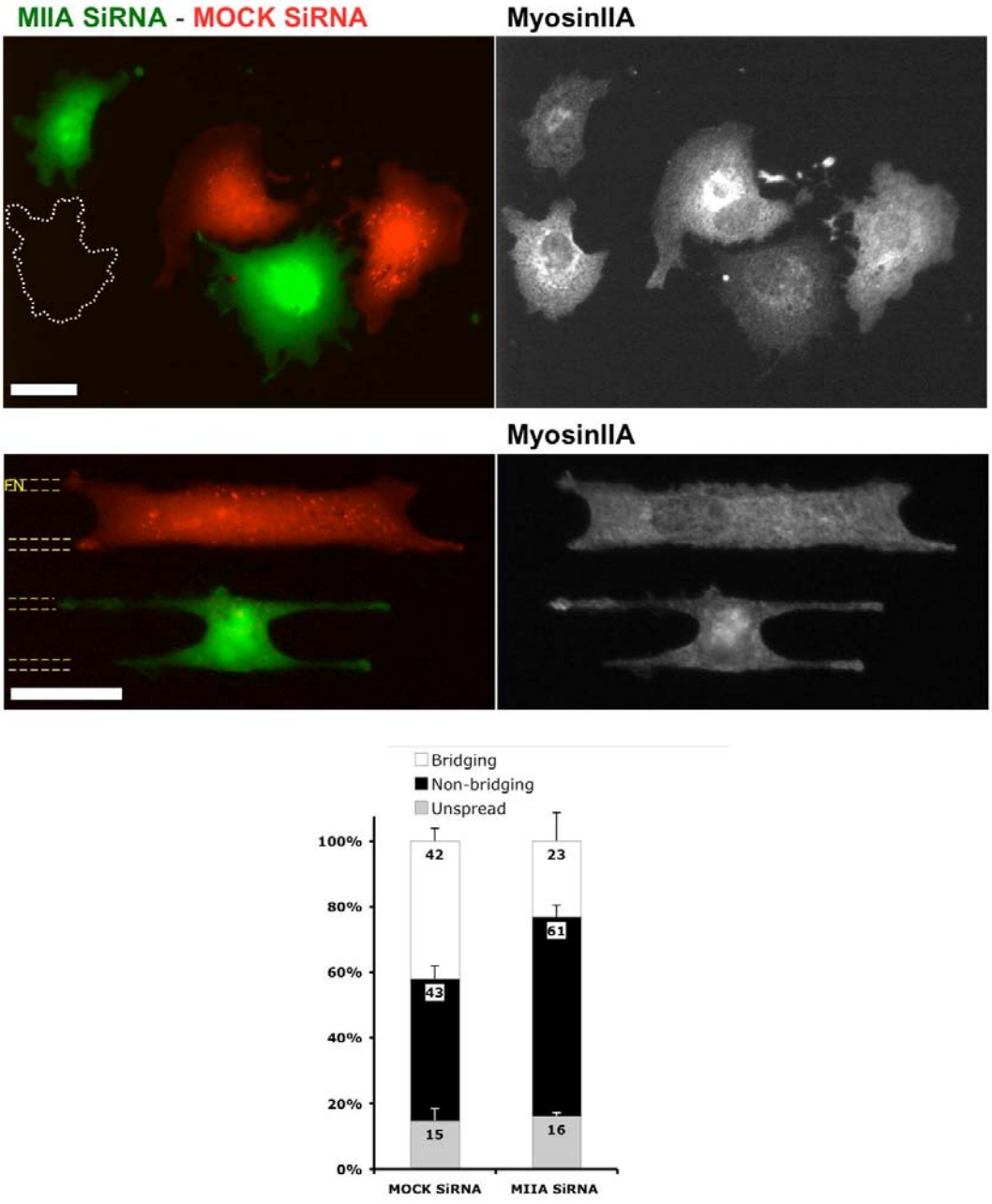

FIGURE S5: **Myosin IIA depletion in MEFs.** Fluorescence image of MEFs either co-transfected with GFP and MIIA siRNA plasmids, or co-transfected with mCherry and Mock siRNA plasmids, plated for 30 min onto continuous FN coated substrates (top panel) or on micropatterned substrates with FN stripes (middle panel). On the left are shown the merge of the green and red fluorescence channels and on the right, MIIA staining images for the same cells obtained by immunofluorescence (scale bars: 30μm). Bottom panel: Histogram representing the percentage of cells after 30min on FN stripes, which are displaying bridges (white), spread without bridges (black), and unspread (light gray) for respectively, MEFs treated with Mock siRNA and MIIA siRNA. Error bars are sd.

Legends for Videos:

VIDEO 1: **Bridges generated strongest traction forces on the sides of concave edges.** This movie shows the time course of the experiment depicted in Fig. 1 C. It covers a period of about 29 min, during which a cell spread on PDMS force-sensing pillars deflected strongly pillars at the sides of the concave edges. Scale bar = 15 μm. Speed, 150X. (QuickTime; 7.3 MB)

VIDEO 2: **Formation of bridges during initial spreading.** This movie shows the time course of the experiment depicted in Fig. 2 A. It covers a period of about 300 seconds, during which a cell spread regardless of substrate coating until bridges formed (t = 100 s) when the edge become concave above non-adhesive areas. Scale bar = 18 μm. Speed, 100X. (QuickTime; 1.7 MB)

VIDEO 3: **Formation of bridges during initial spreading correlates with actin fibers enrichment and bending above non-adhesive regions.** This movie shows the time course of the experiment depicted in Fig. 2 A (middle panel). It covers a period of about 8 min, during which an EGFP-β-actin transfected cell observed by TIRF microscopy is spreading onto a FN-patterned substrate. Scale bar = 15 μm. Speed, 100X. (QuickTime; 3.4 MB)

VIDEO 4: **Formation of bridges during initial spreading correlates with a myosin-II mediated contraction above non-adhesive regions.** This movie shows the time course of the experiment depicted in Fig. 2 A (lower panel). It covers a period of about 30 min, during which an EGFP-MRLC transfected cell observed by TIRF microscopy is spreading onto a FN-patterned substrate. Scale bar = 15 μm. Speed, 200X. (QuickTime; 4.7 MB).

VIDEO 5: **Bridges extension between adhesive stripes happened through cycles of actin-rich protrusions followed by contraction into myosin II bundles colocalized with the characteristic concave edges.** This movie shows the time course of the experiment depicted in Fig. 2 B. It covers a period of about 20 min, during which a cell transfected with EGFP-MRLC and mRFP-β-actin and observed by TIRF microscopy is extending an already formed bridge along FN stripes. Several cycles are visible through out the movie. Scale bar = 7 μm. Speed, 120X. (QuickTime; 4.1 MB).

VIDEO 6: **α-actinin localization and dynamics in bridges.** This movie shows the dynamics of α-actinin speckles by TIRF microscopy within the bridges of a cell transfected with EGFP-α-actinin. It covers a period of about 8 min, during which PIV analysis of GFP-labeled α-actinin revealed two distinct and coexisting patterns at two different localizations, 1) "contractile" at the concave edges of bridges and 2) "cross-linking" patterns in the body of bridges. Scale bar = 15 μm. Speed, 150X. (QuickTime; 4.5 MB).

VIDEO 7: **MRLC localization and dynamics in bridges.** This movie shows the time course of the experiment depicted in Fig. 3 B. It covers a period of about 12 min, during which localization and recruitment of MRLC in the bridges were followed by TIRF speckles microscopy of EGFP-MRLC. Tracking of GFP-labeled MRLC revealed the same two distinct and coexisting patterns found with α-actinin. Scale bar = 15 μm. Speed, 180X. (QuickTime; 3.3 MB).

VIDEO 8: **Reversible collapse of bridges induced by myosin II inhibition.** This movie shows the time course of the experiment depicted in Fig. 4 A. It covers a period of about 200 min, during which cells first spread onto a FN-patterned substrate (0-50 min), followed by the dramatic collapse of their bridges upon BBI treatment (50-100 min) and the bridges recovery when the drug is washed-out (100-200 min, 2x accelerated). Scale bar = 30 μm. Speed, 300X. (QuickTime; 5.9 MB)

VIDEO 9: **α-actinin dynamics in bridges during blebbistatin treatment.** This movie shows the time course of the experiment depicted in Fig. 5 B. It covers a period of about 50 min, during which we followed dynamics of α-actinin speckles before (0-25 min) and during BBI treatment (25-50 min) by TIRF microscopy in the bridges of a cell transfected with EGFP-α-actinin. Scale bar = 15 μm. Speed, 300X. (QuickTime; 6.4 MB).

VIDEO 10: **FRAP experiments reveal that myosin II activity focuses the actin assembly to the adhesion sites.** This movie shows the time course of the FRAP experiments depicted in Fig. 5 C. It covers a period of about 9-10 min, during which we followed the fluorescence recovery of actin bundles labeled with GFP-β-actin in region 1. GFP-β-actin in actin bundles was photobleached in a square of 12 μm side in the same cell for two different conditions: left panel represents the control case; right panel shows the same cell in a MII-relaxed state using BBI. Scale bar = 8.5 μm. Speed, 5X. (QuickTime; 1.5 MB).

VIDEO 11: **Collapse of bridges induced by inhibiting actin polymerisation with latrunculin A treatment.** This movie shows the time course of the experiment depicted in Fig. 6 A. It covers a period of about 53 min, during which we followed collapse of bridges upon LA treatment in a similar manner than BBI treatment. Scale bar = 30 μm. Speed, 300X. (QuickTime; 4.6 MB).

VIDEO 12: **Tearing and condensation of actin cytoskeleton in bridges induced by inhibiting actin polymerisation with latrunculin A.** This movie shows the time course of the experiment depicted in Fig. 6 B. It covers a period of about 20 min, during which we followed detachment of actin meshwork from the borders of FN stripes in region 1 upon LA treatment. Scale bar = 30 μm. Speed, 200X. (QuickTime; 3.9 MB).

VIDEO 13: **Latrunculin A treatment disrupts in a 2 step process the actin networks in bridges.** This movie shows the time course of the experiment depicted in Fig. 6 C. It covers a period of about 36 min, during which we followed 2 distinct steps during LA treatment: 1-actin network detachment from the FN stripes with rapid actin fibers condensation followed by 2-slow bridge retraction where diffuse actin network remaining condense into asters. Scale bar = 15 μm. Speed, 200X. (QuickTime; 4.1 MB).

VIDEO 14: **MRLC dynamics in cytoplasmic veils during blebbistatin treatment.** This movie shows the time course of the experiment depicted in Fig. 7 A. It covers a period of about 37 min, during which we followed dynamics of MRLC speckles before (0-11.5 min) and during BBI treatment (12-36.8 min) by TIRF microscopy in the bridges of a cell transfected with EGFP-MRLC. Scale bar = 15 μm. Speed, 120X. (QuickTime; 3.3 MB).

VIDEO 15: **MIIA-depletion decreased cells ability to bridge non-adhesive gaps.** This movie shows the time course of the experiment depicted in Fig. 7 C. It covers a period of about 37 min, during which we followed simultaneously spreading of control MEFs (2) and MIIA-depleted cells (4) by siRNA by DIC microscopy. Scale bar = 30 μm. Speed, 150X. (QuickTime; 2.4 MB).